Journal of Advanced Zoology

ISSN: 0253-7214
*Volume **44** Issue **5 Year 2023** Page 1446:**1459***

Detection Of Alzheimer Disease Using Deep Learning

Amira Ben Rabeh[1*], Achraf Ben Miled[2], Aws I. Abueid[3]

[1]SEU Saudi Electronic University, Saudi Arabia*
[2]Computer Science Department, Science College, Northern Border University, Arar, Kingdom of Saudi Arabia
[3]Faculty of Computing Studies, Arab Open University, Amman, Jordan

***Corresponding Author:** Amira Ben Rabeh*
**SEU Saudi Electronic University, Saudi Arabia*

Abstract

Alzheimer's disease (AD) is a progressive disease that deteriorates the brain over time and has no existing cure and eventually leads to death. Its detection remains difficult. We present a deep learning-based technique for detecting Alzheimer's disease in its early stages. We propose a method for identifying the human brain surface in structural Magnetic Resonance Imaging (MRI) images. The combination of Active Contour (AC) and Prior Knowledge (PK) from the MRI is a major contribution in this method. We tested many pre-trained networks (AlexNet, VGG16, ResNet18, ResNet50 and MobileNetV2). We tested our method with the collection of OASIS database brain specialized to analyze Alzheimer MRI with 420 subjects; 210 normal and 210 Mild Cognitive Impairment. The majority of patients are aged between 18 to 96 years. The suggested architecture distinguishes between subjects with Normal Control (NC) and (MCI). The classification using the network ResNet50 achieves an exceptional test accuracy of 96.8%. The experimental findings demonstrate the suggested method's capacity to improve classification performance when compared to state-of-the-art approaches.

Keywords: Alzheimer's Disease, Active Contours, MRI, Normal Control, Mild Cognitive Impairment

Introduction

Alzheimer's disease is a gradual degenerative disease that causes a loss in cognitive ability and memory. Nerve cell death occurs gradually in parts of the brain associated with memory and language. The individual with Alzheimer's disease gradually loses the ability to remember events, recognize objects and people, retain the meaning of words, and exercise judgment[1].
Alzheimer's disease is a progressive neurological illness that first affects memory function before impacting all cognitive skills and eventually leads to death. As the number of patients impacted has grown, early detection has become a priority. If memory issues worsen and other cognitive abilities

decline, the diagnosis is confirmed[2],[3],[4].
Our contributions to this article are:

- A segmentation method based on prior knowledge: we propose a segmentation method applicable on the axial section based on deformable contours and prior knowledge.
- To diagnose Alzheimer's disease early, multiple pre-trained CNN networks (AlexNet, VGG16, ResNet18, ResNet50, and MobileNetV2) were used to classify the brain.

Literature Review and Related Work

D. Chitradevi et al(2021),[5] work depicted in figure1.

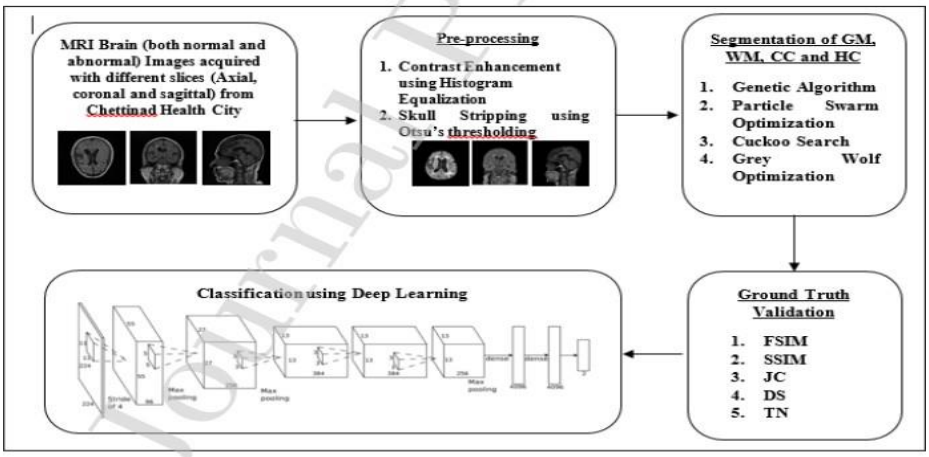

Fig 1. The proposed model by Chitradevi

Figure 2 explains the architecture of network ResNet18[6],[7].

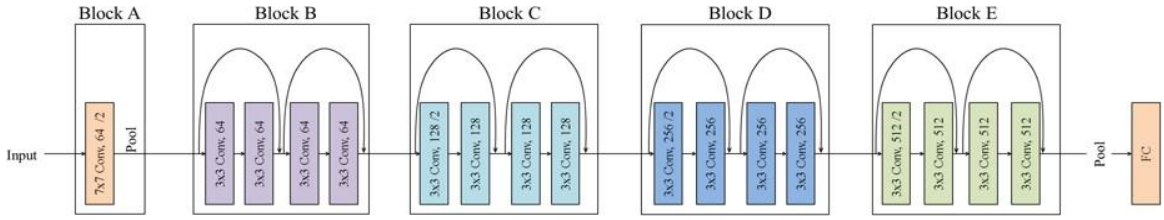

Fig 2. The network ResNet18

AlexNet was the first deep-learning model to win the ImageNet image recognition competition [8],[9]. The figure below explains the architecture of network AlexNet.

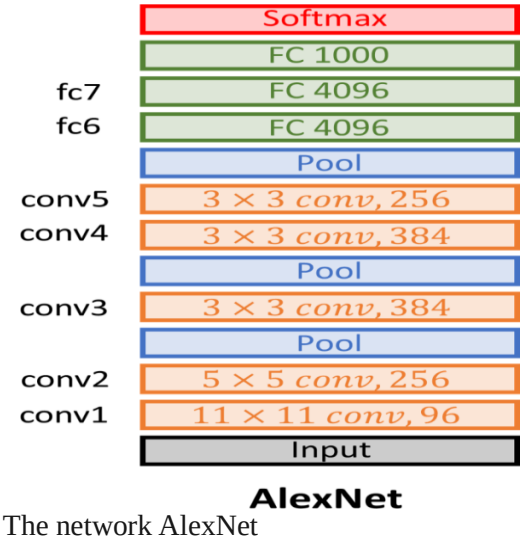

Fig 3. The network AlexNet

Imtiaz Hossain et al. (2020) [10] developed a model to detect Alzheimer's disease using the convolutional neural network MobileNetV2.
Jain et al.(2019) proposed [11] a new computer-assisted diagnosis based on transfer learning via the VGG-16 architecture.

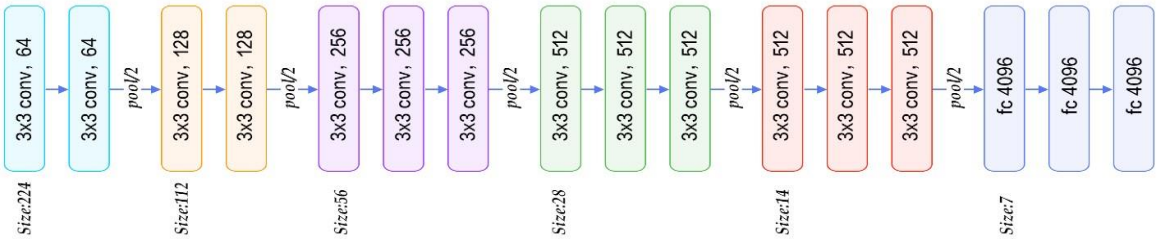

Fig 4. The network VGG-16

Proposed Model

Our method consists of two major components: brain segmentation using Level Set and brain delimitation via Level Set. The second step is deep learning categorization. We put AlexNet, ResNet18, ResNet50, MobileNetv2, and VGG16 through their paces.

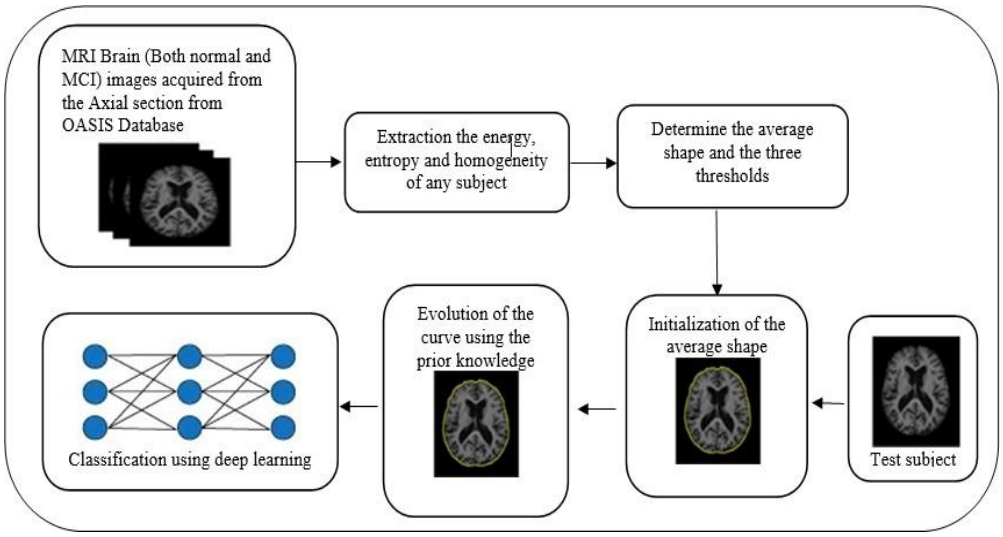

Fig 5. Model of the proposed method

MRI Data set

OASIS (Open Access Series of Imaging Studies) provides brain pictures to scientific community.
The database includes 416 males and females from the OASIS database. The majority of patients are between the ages of18 and 96, they have Normal Control (NC), (MCI), or mild (AD) [12],[13].

3.1 Segmentation using Level Set

The segmentation phase is the most important phase in the Computer Aided Diagnosis System.

Learning Phase

We used the database OASIS database brain; we have 420 samples selected (300 for training and determining the threshold; 120 for testing). Each subject was presented in the axial section, weighted in T1 obtained in the simple digitization sessions. Our expert placed 30 points to extract the brain from each image.

$X=(x_1, y_2, x_2, y_2, ..., x_{30}, y_{30})$

A set of vectors can be used to model the learning base:

$\{X_i\}$ with i=1…N (N number of images of examples)The matrix below illustrates the labeling phase:

With (X_{ij}, Yij) the j^{em} point of the i^{em} shape.

Figure 5.1 presents the labeling phase and the preparation of the learning base [14].

$X_{1,1}$	$Y_{1,1}$	$X_{1,2}$	$Y_{1,2}$	…	…	$X_{1,30}$	$Y_{1,30}$
$X_{2,1}$	$Y_{2,1}$	$X_{2,2}$	$Y_{2,2}$	…	…	$X_{2,30}$	$Y_{2,30}$
…	…	…	…	…	…	…	…
$X_{n,1}$	$Y_{n,1}$	$X_{n,2}$	$Y_{n,2}$	…	…	$X_{n,30}$	$Y_{n,30}$

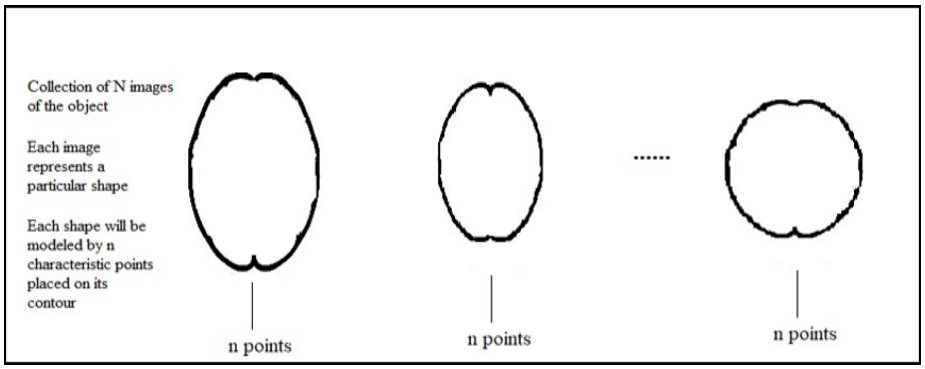

Fig 5.1. Labeling phase and the preparation of the learning base.

Alignment phase

We will first present the steps for aligning two shapes and then the steps for aligning several shapes.

- Alignment of two shapes:

We have two forms:

F1= (x11, y11, x12, y12…, x1n, y1n) (1.1)

F2= (x21, y21, x22, y22…, x2n, y2n)

since we find the shapes sometimes far apart, we need to work on the notion of translation, homothety and rotation.

Our objective is to minimize the distance dF1F2 between the 2 shapes: F1 and F2. We are going to modify F2 in such a way, we are trying to align the two shapes. The expression of the new form is definedby F_{2new}:

F2new=M (S, ɵ) F2+ t (1.2)

Where t is the translation parameter, S is the dilatation and ɵ is the rotation parameter.

-Alignment of multiple shapes.

The algorithm below aligns N shapes:

% Align all shapes relative to first shape %

For i from 2 to N do

Minimize the distance $d_{F1\ Fi\ new}$ between

F_1 and $F_{i\ new}$.Tracer $F_{i\ new}$

End for

While (non-convergence)

% Calculate the average form %

For i from 1 to N do

$F=F+F_i$

End for

F=F/N

% Normalize Average Shape %

Minimize the distance d_{F1F} between F1 and F.

% Alignment of all shapes with respect to the average shape %

For i from 1 to N do

Minimize the distance dF_{Fi} new between

F and $F_{i\ new}$. Tracer Fi new

End for

End While

Average shape or initial contour

For the 200 learning subjects: The inner pixels of the selected contour have been grouped in a matrix.

$X_{1,1}$	$Y_{1,1}$	$X_{1,2}$	$Y_{1,2}$	…	….	$X_{1,n}$	$Y_{1,n}$
$X_{2,1}$	$Y_{2,1}$	$X_{2,2}$	$Y_{2,2}$	…	….	$X_{2,n}$	$Y_{2,n}$
$X_{3,1}$	$Y_{3,1}$	$X_{3,2}$	$Y_{3,2}$	…	….	$X_{3,n}$	$Y_{3,n}$
…	….	…	…	…	…	…	…
$X_{200,1}$	$Y_{200,1}$	$X_{200,2}$	$Y_{200,2}$	…	….	$X_{200,n}$	$Y_{200,n}$

Fig. 5.2 matrix pixels

With (X_{ij},Y_{ij}) the j^{em} point inside the outline of the i^{em} shape.
At each movement of the contour, we compare them with the confidence threshold.

Confidence threshold of energy:

The Second Angular Moment (SAM), also called energy, is a measure that examines the overall homogeneity of the image. Energy = □ □ g

i=1 j=12

i,j

(2)

g_{ij} the value of the pixel located on the i^{th} line and j^{th} column.

Looking through the different samples and the possible variation of energy descriptor, we set thefollowing threshold:

the energy $=avg_{energy} +3/2*var_{energy}$

With energy: the average value of energy.Var energy the variation of the energy.

Confidence threshold of Entropy:

(3)

Entropy is expressed bythe equation given below:

$$Entropy=-\square\ \square\ g_{i,j}\log g_{ij}\quad {}^{Ng}_{i=1}\ {}^{Ng}_{j=1}\ (4)$$

Gij the value of the pixel located on the ith line and j^{th} column.
Looking through the different samples and the possible variation of the entropy descriptor, we set the following threshold:

$threes_{entropy} = avg_{entropy} + var_{entropy}$

With avenergy: the average value of the entropy.varentrophy: the variation of the entropy.

Confidence threshold of homogeneity:

The homogeneity reflects the strong or the weak occurrence of a given pair of pixels, separated by the isometry[15],[16]. Equation is given below:

$$Homogeneity = \sum_{i=1}^{Ng} \sum_{j=1}^{Ng} \frac{g_{i,j}}{1+(i-j)^2}$$

gij the value of the pixel located on the i^{th} line and j^{th} column.(6)

$$thres_{homog} = avg_{homog} + 1/2 * var_{homog}$$

With avghomy: the average value of the homogeneity.

Var_{ho}: the variation of the homogeneity.

Algorithm of learning:

Input: MRI set in the learning base X (Xi,....., Xn)
N: The number of images in the learning base n: The number of characteristic points

Step 1: Extraction of the forms Xi = {Xi1, Xi2,…, Xin} with i = 1…N

Step 2: Alignment of the learning base

Step 3: Generation of the average form

Step 4: Generation of confidence thresholds:

- Energy threshold: $thres_{energy} = avg_{energy} + 3/2 * var_{energy}$
- Entropy threshold: $thres_{entropy} = avg_{entropy} + var_{entropy}$
- Threshold of homogeneity: $thres_{homog} = avg_{homog} + ½ * var_{homog}$

Output:

- Generation of an average form
- Determination of the three thresholds from the learning base.

Phase of contour evolution

These models benefit from picture segmentation by incorporating a global perspective of the shape and structure to be extracted [17],[18] and summarized as follows:

$$F(c1, c2, C) = .longueur(C) + .aire(int(C)) + \lambda_1 \int_{int(C)} |I(x,y) - c1|^2 dxdy + \lambda_2 \int_{ext(C)} |I(x,y) - c2|^2 dxdy$$

Where

$\lambda_1, \lambda_2 > 0$, $\mu > 0$, $\nu > 0$,

Intensity of the standard of Intensity of the standard of deviation inside deviation outside

Algorithm of evolution of the contour:

Input: Input image: test MRI
Average shape
Three thresholds: energy, homogeneity and entropy.
Steps : Evolution of the curve
Stop=false
- **While** (stop ~= true)
  - Evolution of the curvature according to the new function of the energy which is based on the notion of theneighboring pixels and the integration of the prior knowledge.
  - At each iteration, the shape obtained is compared with the energy threshold, the entropy threshold and thehomogeneity Threshold.

If((Energy(F_{new}) > avg_{energy})|| (Entropy (F_{new})> $avg_{entropy}$) || (Homogeneity(F_{new})> avg_{Homog}))
{Stop=true}
Else {% the daily evolution of the curvature% Curvature propagation function based on the principleof the deformable contour and the notion of neighborhood.}}
- **End**

Output: delimitation of the brain

Classification

After the step of segmentation using the deformable model and the prior knowledge. We need a classification step to differentiate between MCI and NC.

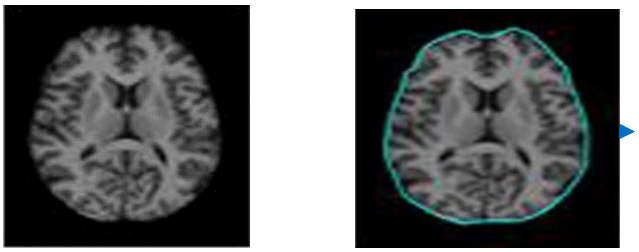

Fig 5.3. The constraint of homogeneity to improve the limit
we employed the homogeneity constraint to increase the limit shown in Figure 5.2

Results and discussion

The results illustrate the benefit of integrating the priorknowledge and generating the average form.

Qualitative assessment

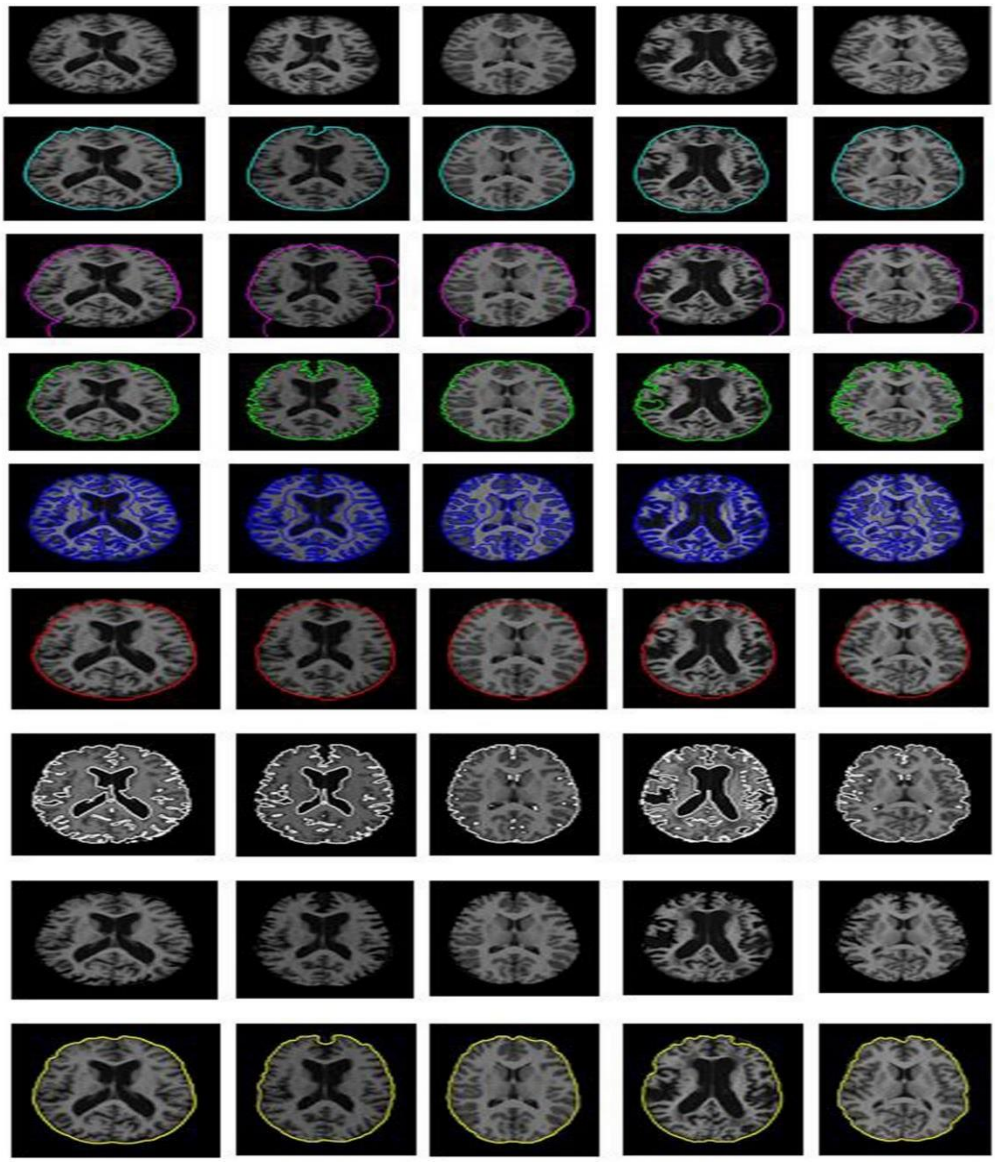

Fig 6. Results of brain delimited using the Level Set methods and our method
The images above show the results of brain extraction, we compared our method with 6 other methods using 5 test subjects [19-22]

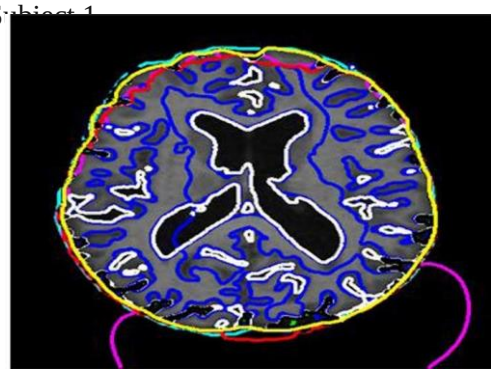

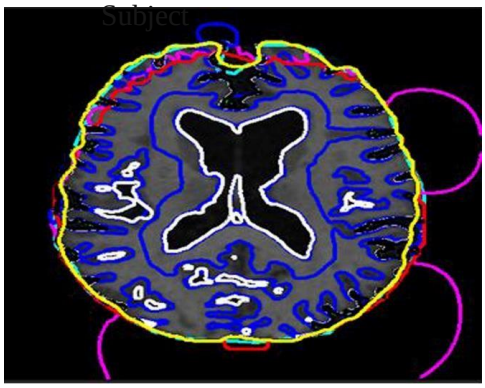

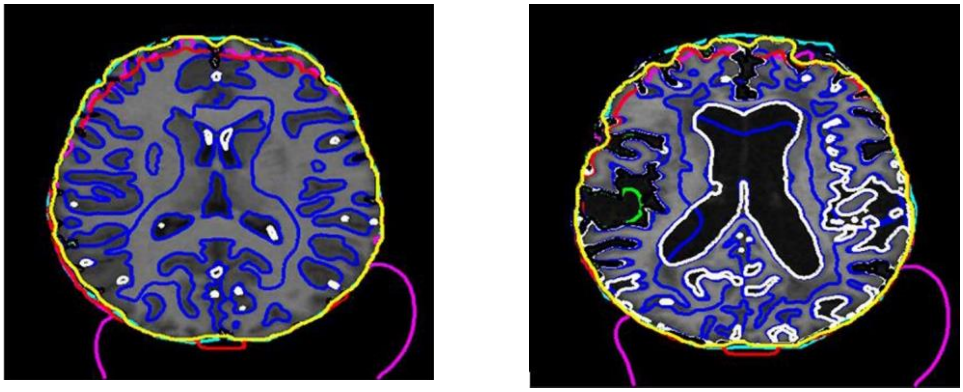

Subject 3 Subject 4

Fig 7. Superposition of the brain delimited results using the Level Set methods and our method for the first subject

Subject 1:
Corresponding results: truth ground (cyan curve), Casselle (pink curve), Chan & Vese (green curve), Chuming-Li (blue curve), Lankton (red curve),Bernard (white curve), Shi (black curve), our method (yellow curve) for the first subject.

Subject 2:
Corresponding results: truth ground (cyan curve), Casselle (pink curve), Chan & Vese (green curve), Chuming-Li (blue curve), Lankton (red curve),Bernard (white curve), Shi (black curve), our method (yellow curve), for the second subject.

Subject 3:
Corresponding results: truth ground (cyan curve),Casselle (pink curve), Chan & Vese (green curve), Chuming-Li (blue curve), Lankton (red curve), Bernard (white curve), Shi (black curve), our method (yellow curve), for the third subject.

Subject 4:
Corresponding results: truth ground (cyan curve), Casselle (pink curve), Chan & Vese (green curve), Chuming-Li (blue curve), Lankton (red curve),Bernard (white curve), Shi (black curve), our method (yellow curve), for the fourth subject.

Quantitative evaluation
It made possible to compensate for the poor quality of the images and to achieve a very good result. We have chosen the Dice coefficient and the Mean Sum of Square Distance (MSSD).
Dice:
The Dice coefficient is a measure of similarity. The coefficient is always in the range of 0 to 1. The formula below summarizes the calculation method:

$$D = \frac{2 * |X \cap Y|}{|X| + |Y|}$$

To calculate the dice coefficient of two samples, it is possible to define X as the terrain truth contour and Y the contour of the test result[17].

MSSD (Mean Sum of Square Distance):
The coefficient MSSD[18] is expressed by this equation:

$$MSSD=\frac{1}{N}\sum_{n=1}^{N} D^2(A,B(x_n))(10)$$

Where:

- A: reference contour
- B: result contour applied our method
- N: length of the resulting curve

$$D_2(A,B(x_n)) = \min_{y \in A} \| y - x \| \quad (11)$$

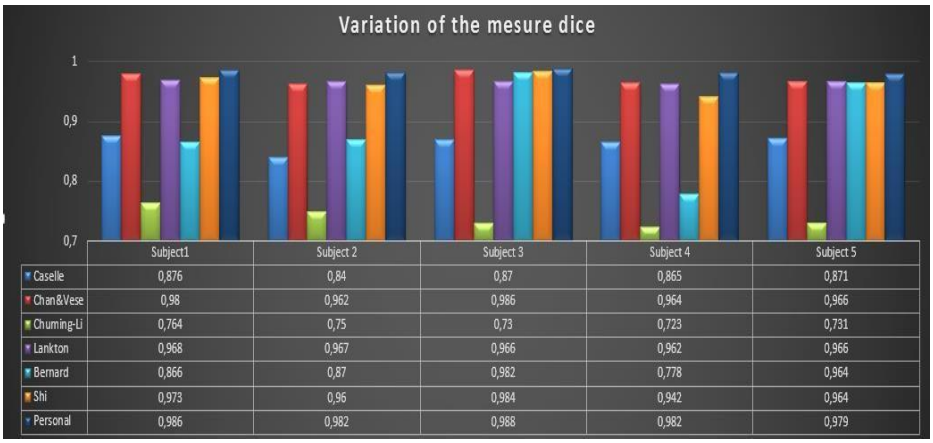

	Subject1	Subject 2	Subject 3	Subject 4	Subject 5
Caselle	0,876	0,84	0,87	0,865	0,871
Chan&Vese	0,98	0,962	0,986	0,964	0,966
Chuming-Li	0,764	0,75	0,73	0,723	0,731
Lankton	0,968	0,967	0,966	0,962	0,966
Bernard	0,866	0,87	0,982	0,778	0,964
Shi	0,973	0,96	0,984	0,942	0,964
Personal	0,986	0,982	0,988	0,982	0,979

Fig 8. Variation of the measure dice

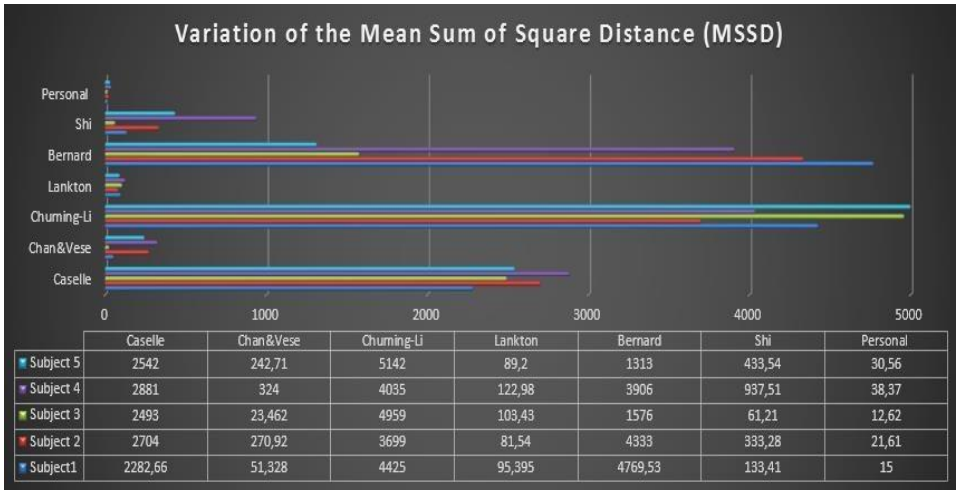

	Caselle	Chan&Vese	Chuming-Li	Lankton	Bernard	Shi	Personal
Subject 5	2542	242,71	5142	89,2	1313	433,54	30,56
Subject 4	2881	324	4035	122,98	3906	937,51	38,37
Subject 3	2493	23,462	4959	103,43	1576	61,21	12,62
Subject 2	2704	270,92	3699	81,54	4333	333,28	21,61
Subject1	2282,66	51,328	4425	95,395	4769,53	133,41	15

Fig 9. Variation of the MSSD.

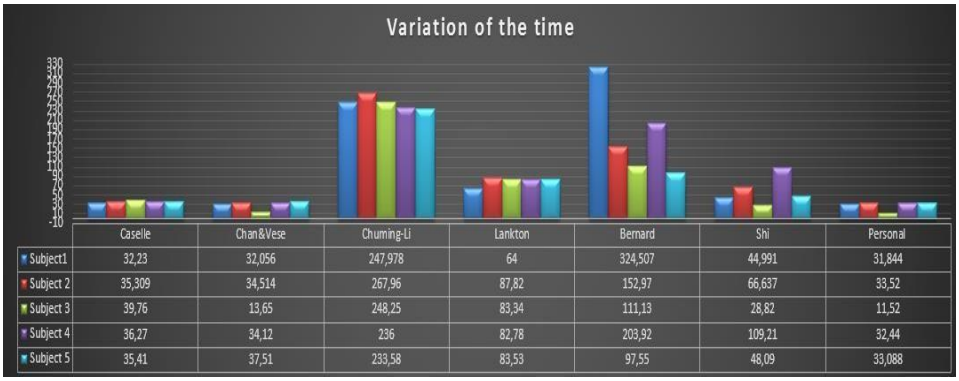

	Caselle	Chan&Vese	Chuming-Li	Lankton	Bernard	Shi	Personal
Subject1	32,23	32,056	247,978	64	324,507	44,991	31,844
Subject 2	35,309	34,514	267,96	87,82	152,97	66,637	33,52
Subject 3	39,76	13,65	248,25	83,34	111,13	28,82	11,52
Subject 4	36,27	34,12	236	82,78	203,92	109,21	32,44
Subject 5	35,41	37,51	233,58	83,53	97,55	48,09	33,088

Fig 10. Variation of the time

We find that our method has values ranging from 0.979 to 0.988 with the best Dice coefficient values, whereas the other methods have values ranging from 0.723 to 0.98.

ResNet50

Fig 11. Result of Convolutional Neuronal Network

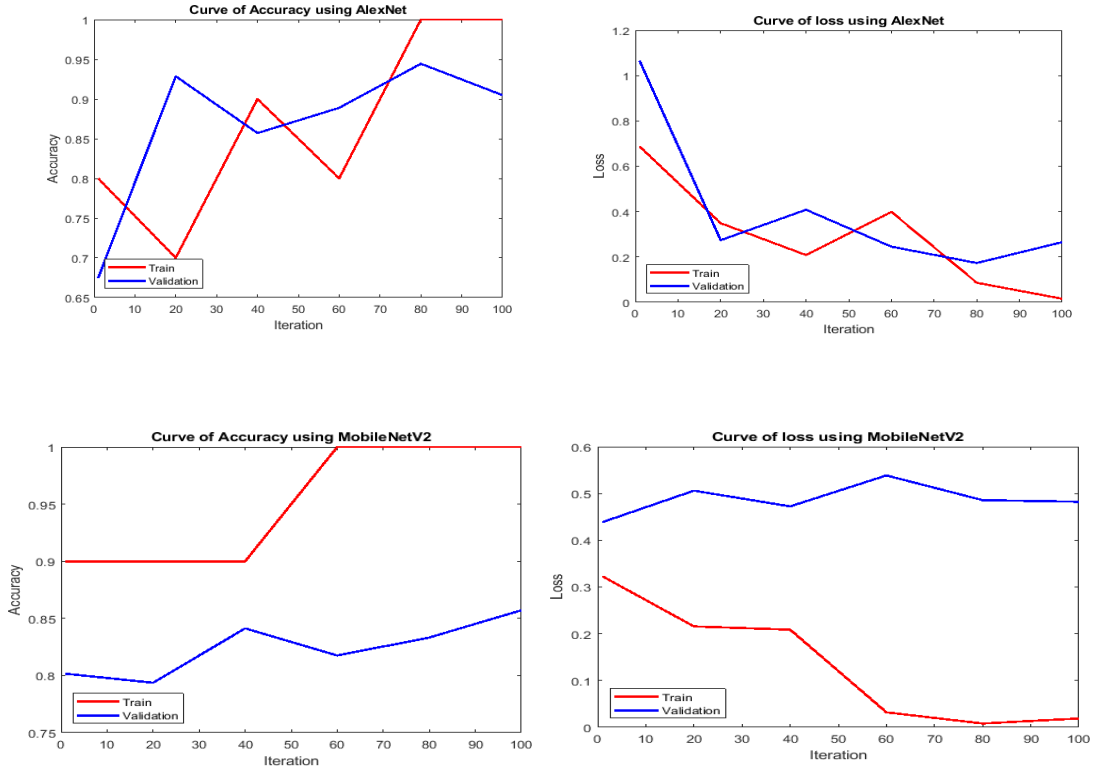

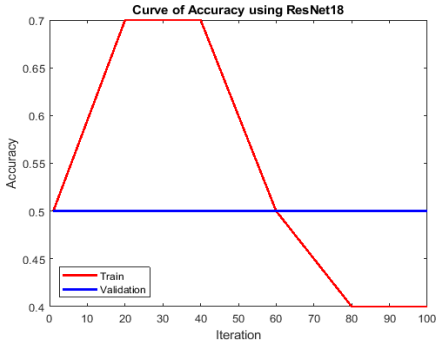
Curve of Accuracy using ResNet18
Accuracy
Iteration
Train
Validation


Curve of loss using ResNet18
Loss
Iteration
Train
Validation

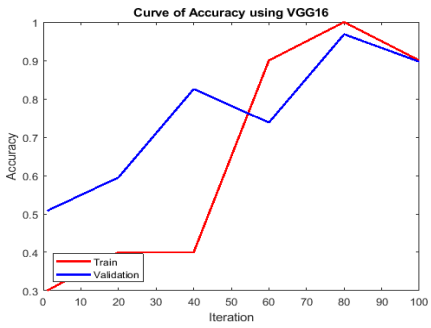
Curve of Accuracy using VGG16
Accuracy
Iteration
Train
Validation

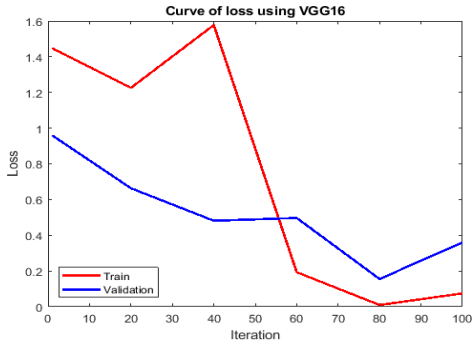
Curve of loss using VGG16
Loss
Iteration
Train
Validation

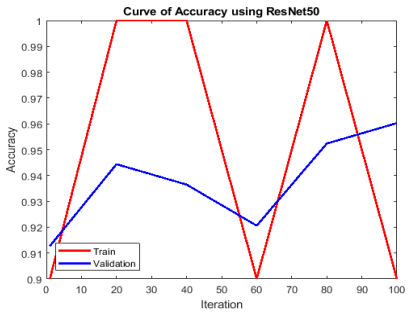
Curve of Accuracy using ResNet50
Accuracy
Iteration
Train
Validation

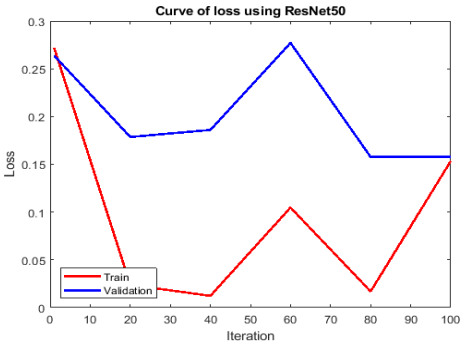
Curve of loss using ResNet50
Loss
Iteration
Train
Validation

Fig 12. Result of CNN
Table 1. Results of our methods and other recent methods

	Training	Validation	Accuracy
Nawaz H et al(2021) **AlexNet**	70	30	90.5%
	80	20	94%
	90	10	88.1%
Emtiaz Hossain etal. (2020) **MobileNetV2**	70	30	92.1%
	80	20	94%
	90	10	95.2%
Farheen Ramzan etal (2020) **ResNet18**	70	30	45.2%
	80	20	47.6%
	90	10	47.6%
Jain et al. (2019) **VGG16**	70	30	89.7%
	80	20	92.9%
	90	10	95.24%
Our method **ResNet50**	70	30	96.8%
	80	20	91.7%
	90	10	92.9%

The accuracy is evaluated in the table above.

Conclusion:

Our model is divided into two parts: brain extraction and classification. The extraction method is based on the Level Set formalism and prior texture information. This effort is related to the same issue of integrating existing information to improve extraction outcomes. In addition, following the brain delineation step, we included a CNN deep learning classification stage to detect Alzheimer's disease at an early stage. We put many pre-trained networks to the test (AlexNet, ResNet18, ResNet50, VGG16, and MobileNetV2). The classification using the network ResNet50 achieves an exceptional test accuracy of 96.8%. We can improve our results and observations by using different databases with more representative cases and learning samples. Expand our work to detect other neurological disorders such as malignancies, Parkinson's disease, and epilepsy.

Funding Statement:

The authors gratefully acknowledge the approval and the support of this research study by grant no. SCIA-2022-11-1278 from the Deanship of Scientific Research at Northern Border University, Arar, K.S.A.

Conflicts of Interest: The authors declare no conflict of interest.

Author Contributions:

All Authors:
They participated in the methodology, Conceptualization, Data collection, and writing the study.

References

1. Kishita, N., Backhouse, T. and Mioshi, E., 2020. Nonpharmacological interventions to improve depression, anxiety, and quality of life (QoL) in people with dementia: an overview of systematic reviews. Journal of geriatric psychiatry and neurology, 33, pp.28-41.
2. Samieri, C., Perier, M.C., Gaye, B., Proust-Lima, C., Helmer, C., Dartigues, J.F., Berr, C., Tzourio, C. and Empana, J.P., 2018. Association of cardiovascular health level in older age with cognitive decline and incident dementia. Jama, 320(7), pp.657-664.
3. Sato, C., Barthélemy, N.R., Mawuenyega, K.G., Patterson, B.W., Gordon, B.A., Jockel-

Balsarotti, J., Sullivan, M., Crisp, M.J., Kasten, T., Kirmess, K.M. and Kanaan, N.M., 2018. Tau kinetics in neurons and the human central nervous system. Neuron, 97(6), pp.1284-1298.
4. Ralph, S.J. and Espinet, A.J., 2018. Increased all-cause mortality by antipsychotic drugs: updated review and meta-analysis in dementia and general mental health care. Journal of Alzheimer's disease reports, 2(1), pp.1-26.
5. Chitradevi, D. and Prabha, S., 2020. Analysis of brain sub regions using optimization techniques and deep learning method in Alzheimer disease. Applied Soft Computing, 86, p.105857.
6. Kundaram, S.S. and Pathak, K.C., 2021. Deep learning-based Alzheimer disease detection. In Proceedings of the Fourth International Conference on Microelectronics, Computing and Communication Systems: MCCS 2019 (pp. 587-597). Springer Singapore.
7. Ramzan, F., Khan, M.U.G., Iqbal, S., Saba, T. and Rehman, A., 2020. Volumetric segmentation of brain regions from MRI scans using 3D convolutional neural networks. IEEE Access, 8, pp.103697-103709.
8. Krizhevsky, A., Sutskever, I. and Hinton, G.E., 2012. Imagenet classification with deep convolutional neural networks. Advances in neural information processing systems, 25.
9. Russakovsky, O., Deng, J., Su, H., Krause, J., Satheesh, S., Ma, S., Huang, Z., Karpathy, A., Khosla, A., Bernstein, M. and Berg, A.C., 2015. Imagenet large scale visual recognition challenge. International journal of computer vision, 115, pp.211-252.
10. Hussain, E., Hasan, M., Hassan, S.Z., Azmi, T.H., Rahman, M.A. and Parvez, M.Z., 2020, November. Deep learning based binary classification for alzheimer's disease detection using brain mri images. In 2020 15th IEEE Conference on Industrial Electronics and Applications (ICIEA) (pp. 1115-1120). IEEE.
11. Jain, R., Jain, N., Aggarwal, A. and Hemanth, D.J., 2019. Convolutional neural network based Alzheimer's disease classification from magnetic resonance brain images. Cognitive Systems Research, 57, pp.147-159.
12. Lehmann, E.L., 2012. An interpretation of completeness and Basu's theorem. Selected Works of EL Lehmann, pp.315-320.
13. Ardekani, B.A., Figarsky, K. and Sidtis, J.J., 2013. Sexual dimorphism in the human corpus callosum: an MRI study using the OASIS brain database. Cerebral cortex, 23(10), pp.2514-2520.
14. Gower, J.C., 1975. Generalized procrustes analysis. Psychometrika, 40, pp.33-51.
15. Haralick, R.M., Shanmugam, K. and Dinstein, I.H., 1973. Textural features for image classification. IEEE Transactions on systems, man, and cybernetics, (6), pp.610-621.
16. Haralick, R.M., 1979. Statistical and structural approaches to texture. Proceedings of the IEEE, 67(5), pp.786-804.
17. Osher, S. and Sethian, J.A., 1988. Fronts propagating with curvature-dependent speed: Algorithms based on Hamilton-Jacobi formulations. Journal of computational physics, 79(1), pp.12-49.
18. Chan, T.F. and Vese, L.A., 2001. Active contours without edges. IEEE Transactions on image processing, 10(2), pp.266-277.
19. Caselles, V., Kimmel, R. and Sapiro, G., 1997. Geodesic active contours. International journal of computer vision, 22, pp.61-79.
20. Caselles, V., Catté, F., Coll, T. and Dibos, F., 1993. A geometric model for active contours in image processing. Numerische mathematik, 66, pp.1-31.
21. YEZZI, A., 1998. A geometric snake model for segmentation. IEEE Imag, Proc., 7, pp.433-443.
22. Dice, L.R., 1945. Measures of the amount of ecologic association between species. Ecology, 26(3), pp.297-302.
23. Nawaz, H., Maqsood, M., Afzal, S., Aadil, F., Mehmood, I. and Rho, S., 2021. A deep feature-based real-time system for Alzheimer disease stage detection. Multimedia Tools and Applications, 80, pp.35789-35807.